

# A STUDY ON LEVEL OF RELIABILITY FOR THE ANGULAR DISTRIBUTION ANALYSIS

**Kamaljeet Singh**

NET Qualified

**Declaration of Author:** I hereby declare that the content of this research paper has been truly made by me including the title of the research paper/research article, and no serial sequence of any sentence has been copied through internet or any other source except references or some unavoidable essential or technical terms. In case of finding any patent or copy right content of any source or other author in my paper/article, I shall always be responsible for further clarification or any legal issues. For sole right content of different author or different source, which was unintentionally or intentionally used in this research paper shall immediately be removed from this journal and I shall be accountable for any further legal issues, and there will be no responsibility of Journal in any matter. If anyone has some issue related to the content of this research paper's copied or plagiarism content he/she may contact on my above mentioned email ID.

## **ABSTRACT**

*In this current study, some research work is done on angular distribution of gamma rays. To check the level of reliability for the angular distribution analysis in the current work, tests were made with transitions of known multi polarity. The measurement of the angular distribution of a  $\gamma$ -ray transition can help to determine the multi polarity of the transition and consequently the spins of the excited nuclear states. The nuclei produced in a fusion-evaporation reaction, for example, are aligned with the angular momentum vector perpendicular to the beam direction. It is therefore possible to obtain an anisotropic angular distribution. If there is no preferred direction, the angular distributions are isotropic.*

**KEYWORDS:** Angular, Distribution, gamma, rays

## **INTRODUCTION**

The initial alignment of the nucleus can be smeared out by the emission of evaporated particles. The angular distribution formula is given by

$$W(\theta) = \sum A_k P_k(\cos \theta)$$

where  $W(\theta)$  is the  $\gamma$ -ray intensity measured at angle  $\theta$  to the beam direction. In the case

of  $\gamma$ -ray emissions, where the parity is conserved, only  $k$ =even numbers are considered, less than or equal to  $2l$  where  $l$  is the angular momentum taken away by the emitted photon.  $P_k(\cos \theta)$  are the standard Legendre polynomials and the  $A_k$  are the angular distribution coefficients. The  $A_k$  value depends on the  $m$ -population distribution and the  $I_{\pi}$  values of the initial

and final states. For an electric dipole transition  $\Delta L = 1$ , or magnetic dipole transition,  $W(\theta)$  will be given by

$$W(\theta) = A_0(1 + A_2P_2(\cos \theta))$$

where  $P_2(\cos \theta) = 1/2 (\cos 2\theta - 1)$  and  $A_0$  is the “true” intensity. For an electric quadrupole ( $E_2$ ) transition  $\Delta L = 2$ , or magnetic quadrupole transition ( $M_2$ ), the angular distribution will be given by

$$W(\theta) = A_0(1 + A_2P_2(\cos \theta) + A_4P_4(\cos \theta))$$

where  $P_4 = 1/8 (35 \cos^4 \theta - 30 \cos^2 \theta + 3)$ .

Experimentally, the dependence of the  $\gamma$ -ray intensity versus the polar angle of the  $\gamma$  detectors will be directly measured.

The Chico detector consists of 20 separate trapezoidal Parallel Plate Avalanche Counters. The essential elements of each PPAC comprise a thin film anode, segmented in two unequal parts, plus a cathode circuit board which is segmented into  $1^\circ$  wide traces of constant polar angle  $\theta$ . There are two identical hemispherical assemblies, each of which houses 10 of the PPACs arranged in a truncated cone coaxial with the beam direction. Figure shows one hemisphere of the Chico detector installed in one half of Gamma sphere. The forward assembly due to the forward focused

reaction kinematics, has an active  $\theta$  range from  $12^\circ$  to  $85^\circ$ . An individual PPAC covers an azimuthal width of  $28^\circ$  and there is a dead region of  $8^\circ$  in  $\phi$  between each of the PPACs. For the set-up including both hemispheres, this provides  $280^\circ$  of  $\phi$  coverage for both the forward and backward assemblies. The total angular coverage is approximately  $2.8\pi$  sr, corresponding to about 69% of the total solid angle.

Chico has been designed to measure the azimuthal  $\phi$  and the polar  $\theta$  angles with respect to the beam direction of the scattered nuclei, and the Time-Of-Flight difference. The azimuthal angle  $\phi$  is measured using the segmentation of the anodes. To measure  $\phi$  a “binary” scheme was implemented. The anodes are segmented into two sections covering  $1/3$  and  $2/3$  of the total  $\phi$  angle subtended by the individual PPACs. Chico is used mostly for binary reactions, therefore two-body kinematics demands that the scattered target and beam-like fragments are coplanar to first order note that the emission of light particles, such as neutrons, will shift the fragments slightly out of plane.

As a result of using a thin target, the beam and target-like reaction fragments, BLFs and TLFs respectively, produced in the binary reaction, could be detected using Chico in

coincidence with the  $\gamma$  rays emitted by the nuclei of interest. The  $\Delta$ TOF measured between the detection of the two fragments and the angular information directly given by the recoil detector allows the separation of the BLFs and TLFs. Figure shows the separation between the two binary partners, with the most intense peak lying in the vicinity of the grazing angle which for this particular reaction occurs at the same laboratory angle,  $50^\circ$ , for both the TLFs and BLFs.

Angular correlation of the two coplanar scattered nuclei detected in two opposing PPACs. Figures show a cut-off at  $20^\circ$  as a result of the use of a mask to stop the high counting rate at low angles. The reduction in counts in these spectra at  $60^\circ$  occurs as a result of a support rib in the pressure window of Chico and could be used for internal angular calibration purposes. Figure shows that at low angles for the BLFs distribution and at more backward angles in the case of the TLFs the statistics decrease abruptly. This does not happen as a result of the reaction mechanism. This effect happens since the TLF recoils at high angles have a low velocity. These recoils do not always get through the pressure window of Chico and therefore the detection efficiency of Chico decreases abruptly at those angles for

TLFs. To explain why the efficiency is also very low for BLFs at low angles, even though these recoils have a large velocity we recall that the master trigger condition in the experiment required two recoils to be detected in Chico. The TLFs that are detected at large angles are correlated with the BLFs at low angles therefore if the TLF recoil at large angle is not detected, then the event is not accepted with the direct consequence of efficiency lost for BLFs low angles and TLFs.

## RESEARCH STUDY

In order to extract some limited information with regard to the multi polarities of the transitions above the 3357 keV isomer,  $\gamma$ -ray angular distributions for these  $\gamma$  rays have been measured. A  $\gamma$  delayed –  $\gamma$  prompt –  $\theta$  ring cube was constructed to investigate the angular distributions of prompt  $\gamma$  rays with respect to the beam-target reaction plane. Rings of Gamma sphere detectors located at angles of  $\theta$ :  $34.5^\circ$ ,  $59.4^\circ$ ,  $79.9^\circ$ ,  $90.0^\circ$ ,  $103.4^\circ$ ,  $131.4^\circ$  and  $155.5^\circ$  with respect to the beam direction were used to compare prompt  $\gamma$ -ray intensities. The angle-gated intensities for each ring were corrected for their respective  $\gamma$ -ray detection efficiencies as determined from standard  $^{152}\text{Eu}$  and  $^{133}\text{Ba}$

calibration sources placed at the target position.

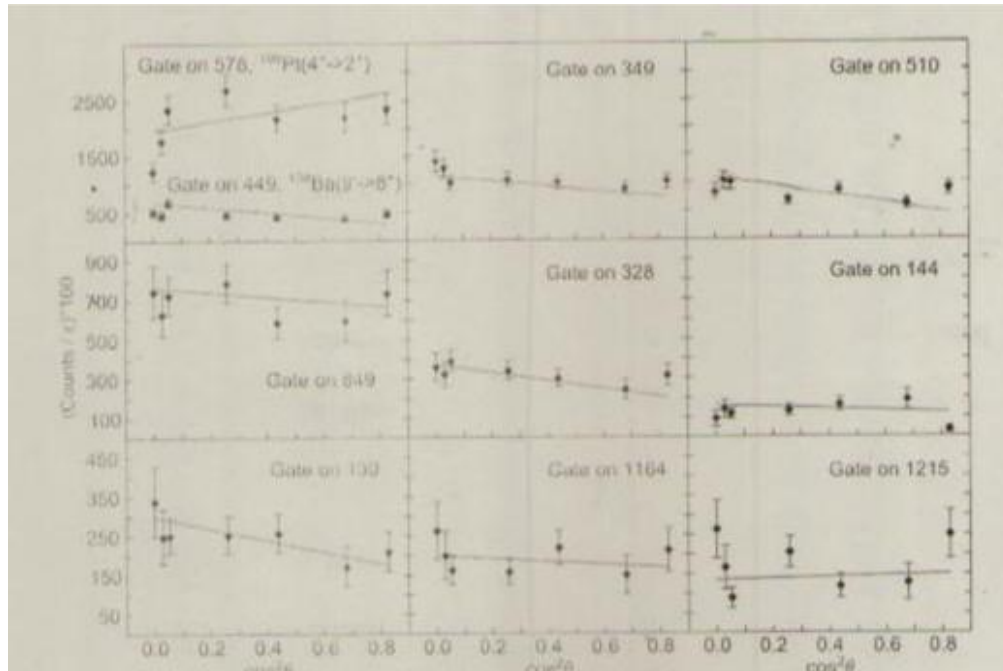


Figure : Gamma-ray angular distributions. The top-left panel shows angular distributions for known transitions,  $^{198}\text{Pt} (4^+ \rightarrow 2^+)$  (E2 transition) and  $^{138}\text{Ba} (9^- \rightarrow 8^+)$  (E1 transition), the other panels show the angular distributions for the  $\gamma$  rays above the  $10^+$  isomer in  $^{136}\text{Ba}$ .

The  $\gamma$ -ray angular distribution method for deep inelastic collisions has been used previously with thick targets to obtain limited information about the multi polarities of the emitted  $\gamma$  rays. However, as discussed by Zhang , the alignment of the products from such binary collisions is clearly much reduced compared to highly aligned fusion-evaporation reactions. Natively this is what one would expect since the angular momentum of the initial system formed is shared between the two fragments.

The results from two known prompt transitions are shown in Fig. for  $^{198}\text{Pt} (4^+ \rightarrow 2^+)$  578 keV, E2 transition and  $^{138}\text{Ba} (9^- \rightarrow 8^+)$  449 keV, E1 transition. The angular distribution coefficients  $A^2$  were deduced to be  $A^2 = 0.21 \pm 0.18$  and  $A^2 = -0.18 \pm 0.14$  respectively for these transitions. These angular distributions are consistent with previous findings, supporting the current analysis, at least at the  $1\sigma$  level. The fitted curves for the prompt  $\gamma$  rays above the proposed  $10^+$  isomer in  $^{136}\text{Ba}$  are shown in Fig. The angular distribution coefficients  $A_2$

the  $A_4$  coefficient is neglected in the fit found from fitting the slope of the intensities as a function of  $\cos^2 \theta$  are listed in Table . The spin and parity assignments for the states identified above the isomer are somewhat problematic due to the significant uncertainties in the measured angular distributions. These result in making most values consistent with no measurable anisotropy at the  $2\sigma$  level. However, the data suggests that the 349 keV is consistent with a dipole decay at the  $1\sigma$  level.

### ANALYSIS

Assuming conservation of linear angular momentum for the scattered beam and target

$$\cos\theta = \sin \theta_R \sin \theta \cos \varphi_R \cos \varphi + \sin \varphi_R \sin \varphi + \cos \theta_R \cos \theta$$

where  $\theta_R$  and  $\varphi_R$  are the scattering angles of the recoils and  $\theta$  and  $\varphi$  are the detection angles of the  $\gamma$  rays in Gamma sphere. The polar angle  $\theta$  for Gamma sphere are listed in Table. The  $\gamma$ -ray energies as measured in the laboratory frame can thus be Doppler corrected for the BLFs or TLFs. Note that in each case only the  $\gamma$  rays emitted by the nuclei for which the Doppler correction is made are enhanced in the resulting spectrum, while those with the incorrect Doppler correction will be smeared out. This technique provides a powerful way of separating the  $\gamma$  rays emitted from the BLFs and TLFs. Figure shows the prompt  $\gamma$  rays which were measured to be within  $\Delta t = \pm 45\text{ns}$  of the master trigger, with no Doppler correction applied.

**Table : Polar angle  $\theta$  for the different rings of the  $\gamma$ -array Gamma sphere and the number of working detectors in each ring.**

$\theta(\text{degrees})$	# detectors	$\theta(\text{degrees})$	# detectors
<b>Forward angles</b>		<b>Backward angles</b>	
17.27	1	99.29	5
31.72	5	100.81	5
37.38	4	110.18	10
50.07	9	121.72	5

58.28	5	129.93	10
69.82	10	142.62	5
79.19	5	148.28	5
80.71	4	162.73	5
90.00	9		

the same spectra Doppler corrected for BLFs and TLFs respectively. Note that the BLF Doppler corrected spectrum shows the prompt 349-keV transition which feeds the  $10^+$  isomer in  $^{136}\text{Ba}$  while in the TLF Doppler corrected spectrum the 407-keV transition ( $2^+ \rightarrow 0^+$ ) in  $^{198}\text{Pt}$  can be identified. The low-lying prompt transitions from the  $^{136}\text{Xe}$  beam nucleus e.g.,  $E(2^+ \rightarrow 0^+) = 1313$  keV are not obviously evident in Fig. due to the presence of a low-lying  $I = 6^+$ ,  $t_{1/2} = 3$   $\mu\text{s}$  isomeric state in this nucleus which traps most of the prompt feeding. Figures show delayed  $\gamma$  rays gated in two different time regimes.  $\gamma$  rays emitted within the time range 200 ns to 780 ns, while Fig. shows  $\gamma$  rays within the first 200 ns of the detection of the binary fragments in Chico. The latter shows transitions associated with the low-lying states of  $^{136}\text{Ba}$  the  $2^+ \rightarrow 0^+$  in  $^{198}\text{Pt}$  and the delayed neutron peaks at 596 keV and 691 keV coming from inelastic

neutron scattering excitations of  $^{74}\text{Ge}$  and  $^{72}\text{Ge}$  respectively. The two very intense peaks at 110 keV and 197 keV are due to the  $\gamma$  decay of the  $5/2^+$  state in  $^{19}\text{F}$ , with a half-life  $t_{1/2} = 89.3$  ns which is used in the electrical segmentation process of the HPGe detectors.

### SIGNIFICANCE OF THE STUDY

Since it is not possible to identify event by event the isotope detected in Chico, the exact  $Q$ -value of the reaction cannot be calculated as defined. Instead a pseudo  $Q$ -value can be calculated, according to,

$$Q - \text{value}_{\text{pseudo}} = \frac{P_t^2}{2m_{\text{Pt}}} + \frac{P_p^2}{2m_{\text{Xe}}} - \frac{P_0^2}{2m_{\text{Xe}}}$$

where the specific masses of the scattering BLFs and TLFs have been replaced by the beam  $^{136}\text{Xe}$  and target  $^{198}\text{Pt}$  mass respectively. The momenta  $P_p$  and  $P_t$  are

obtained using Equation In Figure the pseudo Q-value of the reaction is plotted versus the scattering angle  $\theta$  of the BLFs and TLFs. These two plots have some common characteristics. Firstly, the total energy surface that is defined in both cases by a diagonal line going from top-right to bottom-left. This line appears as a result of the energy conservation in the reaction. Thus, in the case of TLFs for more and more inelastic processes, where Q is larger, the scattering angle decreases as a direct consequence. Deep inelastic reactions begin to occur around the grazing angle and for larger laboratory angles in the case of the BLFs and to smaller angles in the case of TLFs. The events that have pseudo Q-values  $\approx 0$  correspond to Coulomb or quasi-elastic channels in the reaction.

## MEASUREMENT OF THE ANGULAR DISTRIBUTION OF GAMMA RAYS RESONANTLY SCATTERED BY $^{182}\text{W}$ NUCLEI

The isotope  $^{182}\text{W}$  was chosen for the first experiment for the following reasons:

(a) The Mossbauer effect for the 100.1 keV gamma line had already been observed by that time with this isotope in traditional transmission geometry.

(b) The effect observed in the studies indicated above was rather large at liquid-nitrogen temperature, and this rendered the experiment simpler since there was no need for employing liquid helium.

(c) Metallic tungsten is not a ferro-magnet and has a cubic body-centered crystal lattice.

(d) It is convenient to fabricate gamma sources irradiating metallic tantalum with reactor neutrons.

The decay scheme for the parent nuclide  $^{182}\text{Ta}$  produced upon neutron absorption by a  $^{181}\text{Ta}$  nucleus is shown in Fig. It was proposed to observe the resonant excitation of the  $2^+$  level of the  $^{182}\text{W}$  nucleus at 100.1 keV. In this case, the process of resonant gamma-ray scattering proceeds via the sequence of  $0^+ \rightarrow 2^+$  and  $2^+ \rightarrow 0^+$   $E^2$  transitions.

A scatterer in the form of a metallic-tungsten plate 0.5 mm thick was arranged in the narrowed part of a Sty- rofoam container, which may be filled with liquid nitrogen. The thickness of the container walls at the scatterer position was about 15 mm. This was sufficient for preventing the formation of ice at the container walls throughout the measurement time



direction by two springs. The vibrator, together with the gamma source and the cuvette filled with liquid nitrogen, were closed from the outside by a lead layer of

thickness sufficient for reducing the external-radiation level to a permissible value. The initial gamma-ray beam came to the scatterer through a lead collimator

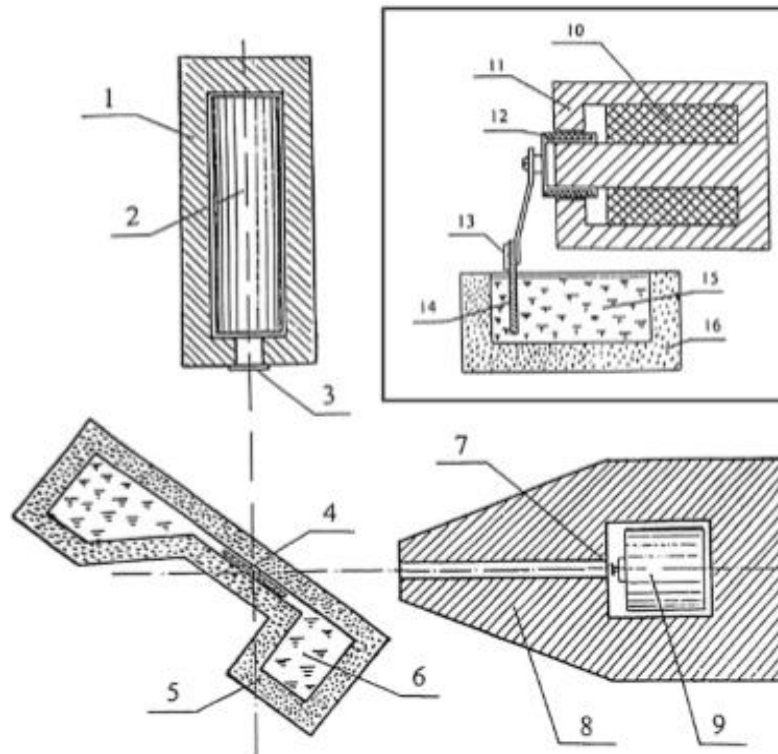


*Fig. Layout of the setup for measuring unperturbed angular distributions of resonantly scattered gamma rays. The inset shows the scheme of fastening of the liquid-nitrogen-cooled gamma source to the movable coil of the electromagnetic vibrator*

## CONCLUSION

The angular momentum transfer in this reaction has been investigated in terms of the average fold versus the scattering angle of the recoils. Some of these plots show a dip at the grazing angle which is understood in terms of quasi-elastic reactions dominating at those angles. The deep-

inelastic reactions take over at angles away from the grazing angle. For nuclei far from the beam or the target, that can only be produced via deep-inelastic reactions no dip shows at the grazing angle. Two different algorithms to extract the energy information are presented, the Moving Window Deconvolution method and an exponential

fitting of the signals. The MWD has been found to be stable, fast and it gives the best energy resolution, 3.5 keV for 1.332 MeV. A tracking algorithm showing results from simulated and experimental data is described. The results obtained for simulated and experimental data for 20 mm position resolution are shown. The P/T hardly improves when the single interaction events are not rejected, but it improves by approximately 70% if the single interaction events are rejected. The efficiency drops by approximately 30% when single events are rejected.

## REFERENCES

- A. De Shalit and H. Feshbach, Theoretical Nuclear Physics Vol 1: Nuclear Structure, John Wiley and Sons Inc., New York (2009).
- E. Der Mateosian and A.W. Sunyar, Atomic Data and Nuclear Data Table 13, 407 (2010).
- F. Rosel et al., Atomic Data and Nuclear Data Table 21, 91 (2012).
- G.F. Knoll, Radiation Detection and Measurement (Wiley) Singapore (2011).
- J.M. Blatt and V.F. Weisskopf, Theoretical Nuclear Physics, John Wiley and Sons Inc., New York (2010).
- J. Kantele, Heavy Ions and Nuclear Structure, vol 5, Nuclear Science Research Conferences Series, B. Sikora and Z. Wilhemi, Harwood, 391 (2012).
- K.S. Krane, Introductory Nuclear Physics, John Wiley and Sons, New York (2008).
- K. Siegbahn, Alpha-, Beta-, and Gamma-Ray Spectroscopy, North-Holland Publishing Company (2010).
- P. Frobrich and R. Lipperheide, Theory of Nuclear Reactions, Oxford, University Press, 2011.